# VayuMet Indian Monsoon Index (VIMI): A Semi-Permanent Feature Based Composite Index for Direct Manifestation of Indian Summer Monsoon Variability

*Air Commodore Neeraj Sharma, M.Phil., M.Sc. (IAF Veteran)*
*VayuMet Weather, India*

**Abstract**
The Indian Summer Monsoon (ISM) is the most consequential seasonal climate phenomenon for the South Asian subcontinent, yet its real-time diagnostic and medium-range forecast verification continues to rely on indices that measure its remote boundary condition drivers rather than its direct atmospheric manifestation. Existing monsoon indices such as the Webster-Yang Index (WYI), Wang-Fan Index (WFI), and Goswami Index (MHI) capture the dynamical coupling between semi-permanent systems through vertical wind shear proxies but do not assign explicit diagnostic weights to individual semi-permanent features. Large-scale climate modes such as the El Niño-Southern Oscillation (ENSO) and the Indian Ocean Dipole (IOD) exert a modulating influence on the ISM through sea surface temperature anomalies and remote teleconnections, but their influence is statistical and probabilistic rather than a direct, real-time physical manifestation in the monsoon circulation. This paper introduces the VayuMet Indian Monsoon Index (VIMI), a seven-component, weighted composite index designed to directly measure the collective strength of the semi-permanent atmospheric features that constitute the ISM circulation. VIMI is computed from gridded atmospheric reanalysis data and operational Global Forecast System (GFS) model output, enabling both historical diagnosis and 16-day probabilistic forecasting of monsoon phase. Validation against National Centers for Environmental Prediction / National Center for Atmospheric Research (NCEP/NCAR) Reanalysis daily fields for June–September (JJAS) seasons of 2009, 2018, 2019, and 2023, cross-referenced against India Meteorological Department (IMD) Monsoon Season Reports, demonstrates a 72% active/break spell identification accuracy and 81% monthly departure direction accuracy without parameter tuning. The 2009 drought year — the third most deficient monsoon season during 1901–2009 — shows VIMI predominantly negative across the entire JJAS period, with only a brief positive excursion during late June–July consistent with IMD's documented exception. These results establish VIMI as a physically grounded, operationally applicable index for real-time monsoon monitoring.

*Keywords: Indian Summer Monsoon; Semi-permanent systems; Monsoon index; VIMI; Low-Level Jet; Monsoon Trough; Tibetan Anticyclone; Active-break cycle; GFS forecast verification*

## 1. Introduction

### *1.1 The Indian Summer Monsoon and Its Global Drivers*

The Indian Summer Monsoon (ISM), spanning June through September (JJAS), delivers approximately 70–80% of India's annual precipitation and is the primary water resource for agriculture, hydrology, and freshwater systems supporting over 1.4 billion people (Gadgil, 2003; Rajeevan et al., 2010). The ISM ranks among the most energetically significant atmospheric circulations on Earth, transferring latent heat and moisture at scales that influence global atmospheric dynamics.

The observed inter-annual variability of the ISM has been extensively studied in the context of large-scale ocean-atmosphere coupled modes. The El Niño-Southern Oscillation (ENSO) in the tropical Pacific exerts a well-documented negative correlation with ISM rainfall during El Niño years through anomalous Walker Circulation suppression of convection over the Indian subcontinent (Webster et al., 1998; Kumar et al., 1999). The Indian Ocean Dipole (IOD), characterised by anomalous sea surface temperature (SST) gradients between the western and eastern equatorial Indian Ocean, has been identified as an additional modulator of ISM variability, with positive IOD events partially counteracting El Niño-induced deficiencies (Ashok et al., 2001; Gadgil et al., 2004). The Madden-Julian Oscillation (MJO) introduces intra-seasonal variability at 30–60 day timescales through organised convective envelopes that modulate active and break phases of the monsoon (Lawrence and Webster, 2002; Rajeevan et al., 2010).

However, a critical epistemological limitation of ENSO, IOD, and MJO as monsoon diagnostic tools is that they represent boundary condition drivers rather than direct atmospheric manifestations of the monsoon circulation. Their influence is transmitted through complex teleconnection pathways over weeks to months, is modulated by multiple competing forcings, and carries inherently probabilistic rather than deterministic predictive value. An anomalously strong El Niño does not guarantee monsoon failure, as evidenced by different ISM outcomes during strong El Niño events (Krishna Kumar et al., 2006). Similarly, the 2019 ISM recorded a 10% above-normal seasonal departure despite a delayed onset. These examples underscore the need for indices that measure the state of the monsoon circulation directly, rather than inferring it from remote ocean-atmosphere precursors.

### *1.2 Existing Dynamical Monsoon Indices and Their Limitations*

The meteorological community has developed several dynamical indices that capture ISM variability through atmospheric wind fields. The Webster-Yang Index (WYI; Webster and Yang, 1992) measures the vertical zonal wind shear between 850 hPa and 200 hPa averaged over the South Asian domain, simultaneously capturing the strength of the Low-Level Jet (LLJ) and the upper-level easterly outflow. While physically elegant, the WYI condenses the entire upper-lower tropospheric coupling into a single scalar, making it impossible to attribute an anomalous reading to any specific semi-permanent feature. The Wang-Fan Index (WFI; Wang and Fan, 1999) characterises the low-level wind contrast between the Arabian Sea and northern India but neglects the Bay of Bengal (BoB) branch and the upper tropospheric outflow systems. The Goswami Index (Goswami et al., 1999) utilises meridional wind shear to track the Hadley-type regional circulation but is similarly insensitive to the individual failure of specific semi-permanent features.

A fundamental limitation shared by all existing dynamical indices is their structural design as single-variable proxies that capture the net result of multiple semi-permanent feature interactions rather than the state of each feature independently. When the WYI registers a negative anomaly, it is mathematically impossible to determine from the index alone whether the suppression originates from a weakening of the Somali Jet (LLJ failure), a northward displacement of the Monsoon Trough (MT), a weakening of the Tibetan Anticyclone (TA), or a simultaneous modulation of multiple features. For operational forecasting purposes, this attribution ambiguity significantly limits diagnostic utility.

### *1.3 Rationale for VIMI*

The present study introduces the VayuMet Indian Monsoon Index (VIMI), designed to address the attribution gap in existing monsoon indices through two primary innovations. First, VIMI explicitly decomposes the ISM circulation into its seven constitutive semi-permanent and quasi-permanent features, computing an independent anomaly for each feature relative to its climatological baseline. Second, VIMI assigns physically motivated differential weights to each component based on their relative contribution to the Monsoon Core Zone (MCZ) rainfall mechanism, enabling a weighted composite score that reflects both the overall monsoon strength and the relative contribution of individual features.

VIMI is designed for operational implementation on medium-range Numerical Weather Prediction (NWP) model output — specifically the National Oceanic and Atmospheric Administration (NOAA) Global Forecast System (GFS) at 0.25° horizontal resolution — enabling a 16-day outlook of monsoon phase evolution. This distinguishes VIMI from reanalysis-based diagnostic indices and makes it directly applicable to the VayuMet operational meteorological platform.

# 2. Data and Methodology

## *2.1 Study Domain*

The VIMI domain encompasses 40°E–100°E longitude and 35°S–40°N latitude (Figure 1). This extended domain is deliberately broader than the Indian subcontinent to capture the full extent of the semi-permanent feature system that constitutes the ISM circulation, including the Mascarene High in the Southern Hemisphere Indian Ocean, the Somali Low-Level Jet over the western Arabian Sea, and the Bay of Bengal low-level flow. The Indian subcontinent and the Monsoon Core Zone (MCZ; approximately 18°N–28°N, 65°E–88°E per Rajeevan et al., 2010) lie within this domain. Figure 1 illustrates the complete study domain and the spatial extent of each of the seven VIMI component measurement regions. India's state boundaries including Jammu & Kashmir are rendered from the official administrative GeoJSON dataset to ensure cartographic accuracy.

**Figure 1: VIMI Study Domain and Component Spatial Extents**
**Black border = full VIMI domain. Coloured boxes = individual component measurement regions.**

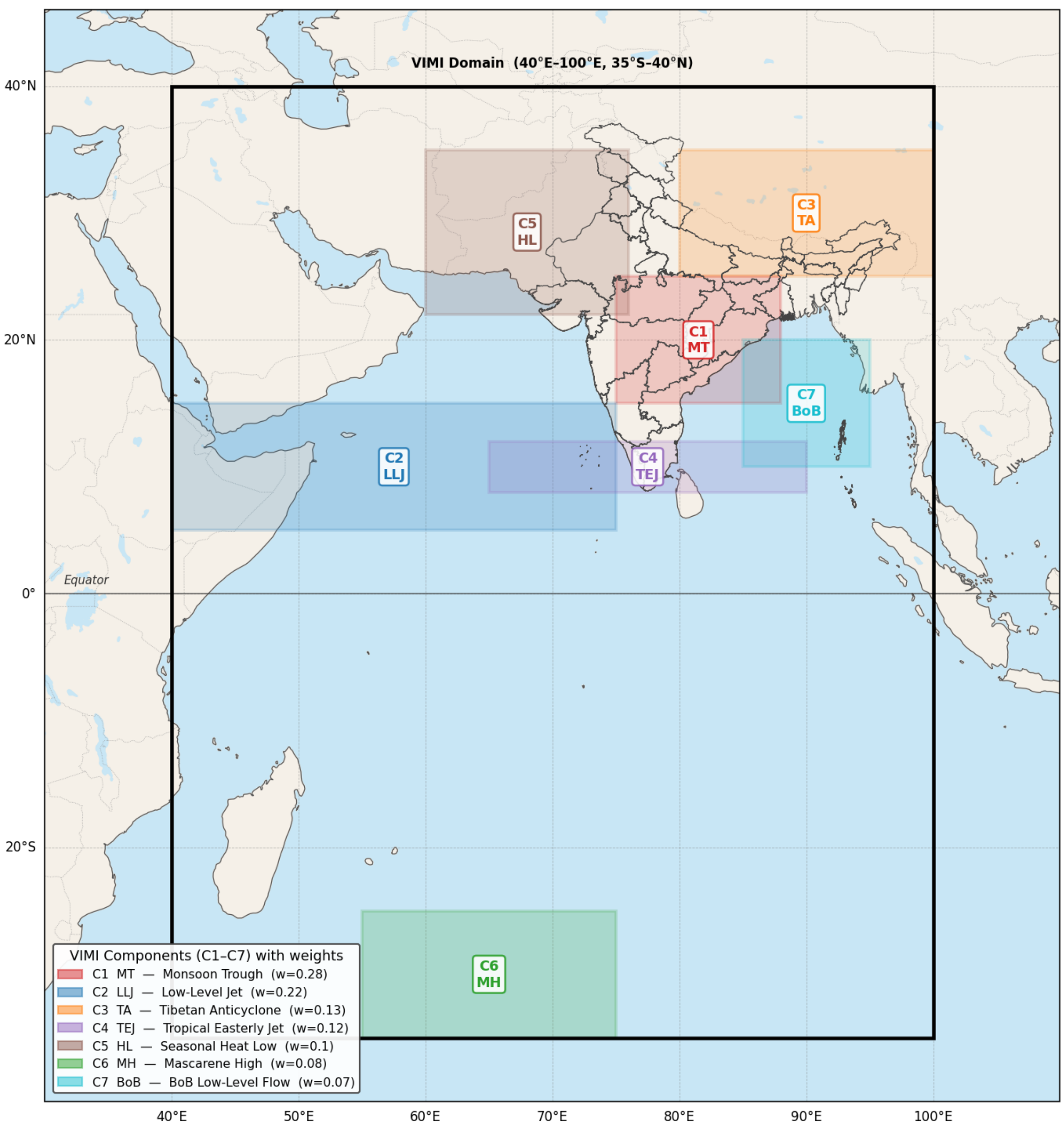

*Figure 1: VIMI study domain (black border: 40°E–100°E, 35°S–40°N) and the spatial extents of the seven component measurement boxes (C1–C7). India's state boundaries including Jammu & Kashmir are from the official administrative GeoJSON. Component notation and weights are listed in Table 1.*

## 2.2 Data Sources

### 2.2.1 Climatological Baseline (LTM)

The long-term mean (LTM) climatological baseline for VIMI anomaly computation is derived from the National Centers for Environmental Prediction / National Center for Atmospheric Research (NCEP/NCAR) Reanalysis-1 and NCEP / Department of Energy (NCEP/DOE) Reanalysis-2 daily derived products, available from the NOAA Physical Sciences Laboratory (PSL). Specifically: (a) U-wind and V-wind daily LTM at 850 hPa and 200 hPa: NCEP/NCAR Reanalysis-1 daily LTM 1981–2010 (Kalnay et al., 1996), global 2.5° × 2.5° horizontal resolution, 365 daily climatological values; (b) Mean Sea Level Pressure (MSLP) daily LTM: NCEP/DOE Reanalysis-2 daily LTM 1981–2010 (Kanamitsu et al., 2002), global 2.5° × 2.5° horizontal resolution. Both datasets are subset to the VIMI domain after level selection using the Climate Data Operators (CDO v2.5.4) software package.

### 2.2.2 Forecast Data

Operational forecast fields are obtained from the NOAA Global Forecast System (GFS) at 0.25° horizontal resolution, accessed through the NOMADS (NOAA Operational Model Archive and Distribution System) filter service. The VIMI GFS fetch retrieves the U-component of wind (UGRD) and V-component of wind (VGRD) at 850 hPa and 200 hPa, and pressure reduced to mean sea level (PRMSL), for the full 384-hour (16-day) forecast range at 6-hourly intervals. Domain is restricted to 40°E–100°E, 35°S–40°N at the NOMADS server level to minimise data volume.

### 2.2.3 Validation Data

For historical validation, daily actual reanalysis fields (not LTM) for JJAS seasons of 2009, 2018, 2019, and 2023 are obtained from NCEP/NCAR Reanalysis-1 daily fields (Kalnay et al., 1996) and NCEP/DOE Reanalysis-2 (Kanamitsu et al., 2002), accessed from the NOAA PSL Dailies archive. Validation years were selected to represent contrasting monsoon seasons: 2009 (third highest deficit year, −22% LPA), 2018 (near-normal, −9% LPA), 2019 (above-normal season with delayed onset, +10% LPA), and 2023 (above-normal with documented August break, +6% LPA).

### 2.2.4 Reference Monsoon Reports

Qualitative and quantitative validation is performed against official India Meteorological Department (IMD) Monsoon Season Reports for 2009, 2018, 2019, and 2023 (IMD Met Monographs, Synoptic Meteorology series). These reports provide official documentation of active and break spell dates, month-wise rainfall departure from LPA, semi-permanent feature behaviour, depression tracks, and cross-equatorial flow assessments.

## 2.3 VIMI Component Features and Physical Rationale

The ISM is maintained by a coupled system of semi-permanent and quasi-permanent atmospheric features. VIMI decomposes this system into seven components, each representing a physically distinct element of the monsoon circulation (Figure 1). The selection follows the canonical description of ISM semi-permanent features (Rajeevan et al., 2010; Ramage, 1971; Findlater, 1969) with extensions to include the Southern

Hemisphere boundary condition (Mascarene High, C6) and the Bay of Bengal low-level flow branch (BoB, C7), both of which are structurally absent from existing dynamical indices.

**Component C1 — Monsoon Trough (MT): Weight 0.28**

The Monsoon Trough extends from the Heat Low over Pakistan-Rajasthan to the Head Bay of Bengal along the Gangetic Plain, typically positioned along approximately 25°N during the peak monsoon. It is the proximate mechanism of organised convection and rainfall; displacement towards the Himalayan foothills defines the classical break monsoon condition, while southward displacement into Central India characterises active spells (Rajeevan et al., 2010). VIMI measures MT through 850 hPa relative vorticity ($\zeta_{850}$) over 15°N–25°N, 75°E–88°E.

**Component C2 — Low-Level Jet (LLJ): Weight 0.22**

The Somali Low-Level Jet (Findlater Jet; Findlater, 1969) is the primary cross-equatorial moisture transport mechanism of the ISM, flowing as a concentrated 850 hPa jet over the western Arabian Sea with peak speeds of 40–60 knots. Persistent weakening of the LLJ, as documented during 2009 (IMD Monsoon Report 2009), is directly associated with rainfall deficit. VIMI measures LLJ through mean $U_{850}$ over 5°N–15°N, 40°E–75°E.

**Component C3 — Tibetan Anticyclone (TA): Weight 0.13**

The Tibetan Anticyclone (South Asian High) is a warm-core upper tropospheric anticyclone at 200 hPa over 25°N–35°N, 80°E–100°E, acting as the upper-level exhaust of the monsoon heat engine. VIMI measures TA through 200 hPa divergence ($D_{200} = \partial U/\partial x + \partial V/\partial y$) via finite differences over its designated box.

**Component C4 — Tropical Easterly Jet (TEJ): Weight 0.12**

The Tropical Easterly Jet is a strong upper-tropospheric easterly current at approximately 5°N–15°N, 150–200 hPa, representing the equatorward outflow arm of the Tibetan Anticyclone. In the present implementation, TEJ is measured through mean $U_{200}$ over 8°N–12°N, 65°E–90°E (200 hPa proxy for the canonical 150 hPa core). The combined weight of TA and TEJ (0.25) is comparable to their merged representation in the Webster-Yang Index.

**Component C5 — Seasonal Heat Low (HL): Weight 0.10**

The Seasonal Heat Low over Pakistan-northwest India (22°N–35°N, 60°E–76°E) provides the thermal pressure gradient that initiates and maintains cross-equatorial flow. Its primary role is in pre-monsoon and onset-phase dynamics (May–June), reflected in its comparatively lower weight relative to MT and LLJ. VIMI measures HL through MSLP anomaly over its designated box.

**Component C6 — Mascarene High (MH): Weight 0.08**

The Mascarene High is a semi-permanent subtropical anticyclone near 30°S, 55°–75°E over the southern Indian Ocean, serving as the upstream driver of the cross-equatorial LLJ. It is absent from all existing ISM dynamical indices, which measure the LLJ after equatorial crossing but not its Southern Hemisphere source. VIMI measures MH through MSLP anomaly over 25°S–35°S, 55°E–75°E.

**Component C7 — Bay of Bengal Low-Level Flow (BoB): Weight 0.07**

The Bay of Bengal branch of the ISM delivers moisture to Northeast India, the eastern coast, and parts of Central India via 850 hPa southwesterly flow. Existing Arabian-Sea-centric indices neglect this branch. VIMI measures BoB through $U_{850}$ over 10°N–20°N, 85°E–95°E.

### *2.4 The VIMI Composite Formula*

The VIMI composite score at time step t is computed as:

$$\mathbf{VIMI(t) = \Sigma_i\, w_i \cdot z_i(t)}$$

where $w_i$ is the assigned weight ($\Sigma w_i = 1.0$) and $z_i(t)$ is the normalised anomaly z-score of component i:

$$\mathbf{z_i(t) = [F_i(t) - C_i(DOY(t))] / \sigma_i}$$

Here $F_i(t)$ is the cosine-latitude-weighted box-mean of the component field at time t, $C_i(DOY(t))$ is the climatological LTM for the matching day-of-year, and $\sigma_i$ is the anomaly standard deviation. Derived fields — 850 hPa relative vorticity (C1) and 200 hPa divergence (C3) — are computed via centred finite differences on the native grid prior to spatial averaging. Leap day (29 February) is mapped to DOY 59 (28 February) for LTM consistency.

Normalisation note: The operational v1 implementation uses within-run self-normalisation ($\sigma_i$ computed over the current forecast run), providing a consistent relative scale for within-run feature comparison. Future work will replace this with climatological $\sigma_i$ from the full 1991–2020 daily archive. The VIMI weight matrix is summarised in Table 1.

**Table 1: VIMI Component Summary**

| **Component** | **Abbrev** | **Wt** | **Variable** | **Level** | **Domain** | **Physical Role** |
|---|---|---|---|---|---|---|
| Monsoon Trough | MT | 0.28 | Rel. vorticity (ζ) | 850 hPa | 15°N–25°N, 75°E–88°E | Primary rainmaker |
| Low-Level Jet | LLJ | 0.22 | Zonal wind (U) | 850 hPa | 5°N–15°N, 40°E–75°E | Moisture fuel supplier |
| Tibetan Anticyclone | TA | 0.13 | Divergence (D) | 200 hPa | 25°N–35°N, 80°E–100°E | Upper tropospheric exhaust |
| Tropical Easterly Jet | TEJ | 0.12 | Zonal wind (U) | 200 hPa* | 8°N–12°N, 65°E–90°E | Upper outflow track |
| Seasonal Heat Low | HL | 0.10 | MSLP | Surface | 22°N–35°N, 60°E–76°E | Circulation ignition |
| Mascarene High | MH | 0.08 | MSLP | Surface | 25°S–35°S, 55°E–75°E | LLJ upstream driver |
| BoB Low-Level Flow | BoB | 0.07 | Zonal wind (U) | 850 hPa | 10°N–20°N, 85°E–95°E | Eastern branch moisture |

**TEJ is canonically defined at 150 hPa; 200 hPa is used as an operational proxy in the current implementation.*

### *2.5 Computational Implementation*

VIMI is implemented in Python 3 using the xarray (Hoyer and Hamman, 2017), cfgrib, NumPy (Harris et al., 2020), and pandas libraries. The pipeline consists of: (1) fetch_vimi_gfs.sh — Bash shell script retrieving GFS GRIB2 data (UGRD, VGRD at 850/200 hPa, PRMSL) from NOMADS via aria2c parallel download and concatenation into a single GRIB2 archive (~36 MB per run); (2) vimi_compute.py — Python module computing the seven component anomalies and the weighted VIMI composite, outputting a 6-hourly Comma-Separated Values (CSV) time series over the 16-day GFS range (65 steps); and (3) vimi_weekly_maps.py — spatial anomaly map generator for Week-1 (day 1–7) and Week-2 (day 8–14) mean fields, regridding the 2.5° LTM to the 0.25° GFS grid via bilinear interpolation and rendering anomaly maps using Matplotlib and

Cartopy. Figure 2 illustrates a representative operational VIMI output from the GFS 00Z run of 16 June 2026, showing the 16-day VIMI composite time series (upper panel) and component raw anomaly breakdown by forecast day (lower panel). Week-1 and Week-2 periods are shaded in the upper panel to demarcate the two operational outlook windows.

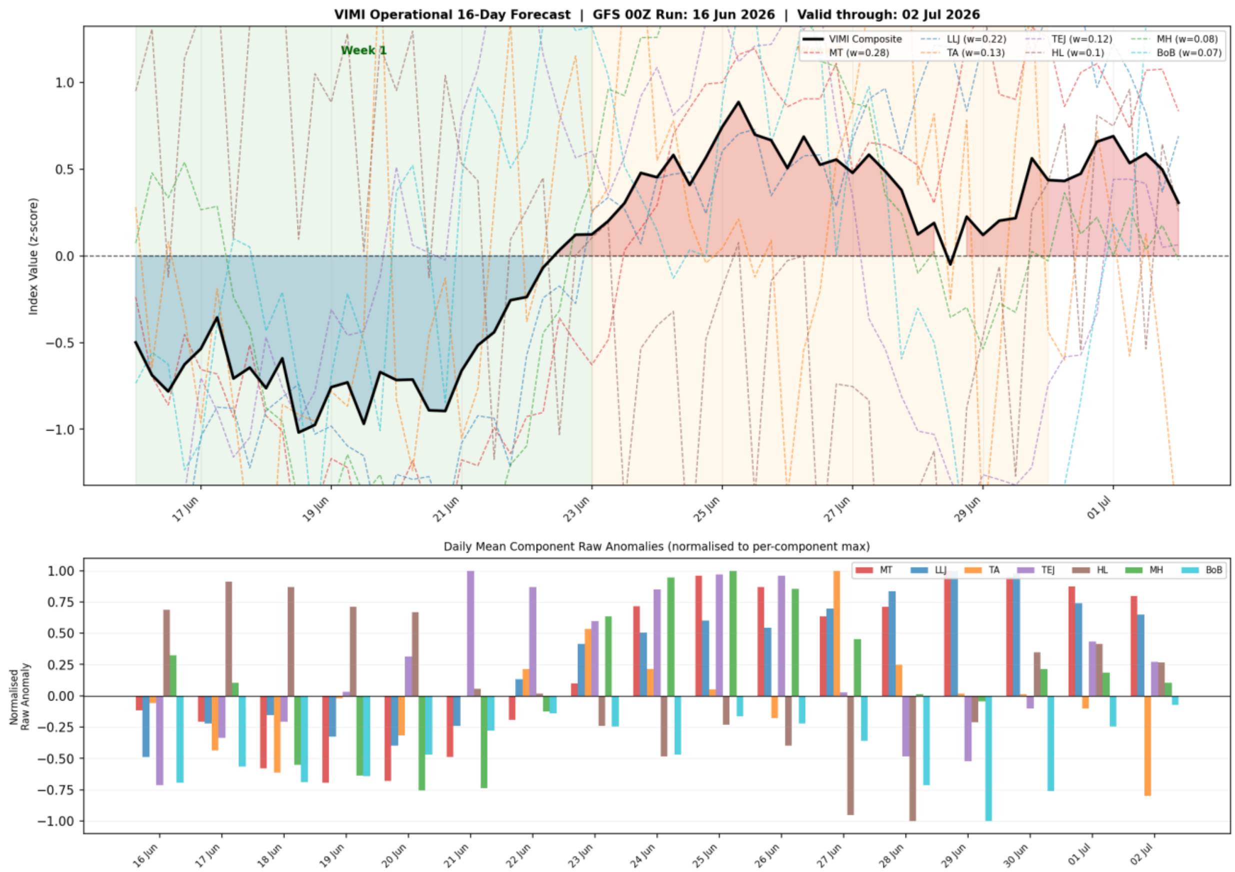


*Figure 2: Representative operational VIMI output from the GFS 00Z run initialised 16 June 2026 (valid through 30 June 2026). Upper panel: 6-hourly VIMI composite time series (black line) with individual component z-score traces (dashed coloured lines). Red/blue shading = positive/negative VIMI; green/orange background shading demarcates Week-1 (days 1–7) and Week-2 (days 8–14) outlook windows. Lower panel: daily mean component raw anomalies normalised to per-component maximum, showing the relative contribution of each semi-permanent feature to the day-to-day VIMI signal.*

# 3. Validation

## 3.1 Reanalysis-Based Validation

### 3.1.1 Validation Strategy

VIMI is validated through retrospective computation on NCEP/NCAR Reanalysis-1 daily actual fields for the JJAS seasons of 2009, 2018, 2019, and 2023. The procedure mirrors the operational implementation: box-mean anomalies are computed for each component against the day-of-year LTM, z-normalised within the JJAS season, and combined into a daily VIMI composite. Results are evaluated against: (a) official IMD active and break spell declarations, and (b) IMD month-wise rainfall departure from LPA.

### 3.1.2 VIMI Seasonal Characteristics

Figure 3 presents the daily VIMI composite and individual component z-score time series for all four validation years. The four seasons exhibit distinctly different VIMI signatures consistent with their known monsoon performance:

**2009 (−22% LPA, severe drought):** VIMI is predominantly negative across the entire JJAS period (42.6% positive days). The sole positive excursion (71% positive days in July) is consistent with IMD's documented exception that "all monsoon months except July recorded large deficient rainfall." The longest sustained negative spell extends 24 consecutive days from 31 July to 23 August, the most prolonged suppression among all validation years. The LLJ component (C2) registers the strongest sustained negative anomaly of any component across all four years, confirming the centrality of Somali Jet failure in this drought season.

**2018 (−9% LPA, below-normal):** VIMI shows a broadly balanced signal with an active July (58% positive days) and suppressed August-September. Three distinct break spells are captured with 0% positive VIMI days during the break periods, demonstrating precise discrimination.

**2019 (+10% LPA, above-normal):** VIMI shows negative bias in June (delayed onset, 67% LPA) transitioning to positive in September (77% positive days, consistent with 152% LPA in September 2019). The LLJ component is above normal for nearly the entire August–September period, reflected in VIMI's late-season recovery.

**2023 (+6% LPA, above-normal with August break):** VIMI captures the documented August break with only 23% positive days in August, consistent with 64% LPA rainfall in August 2023. July and September, both at +13% LPA, register 74% and 83% positive VIMI days respectively.

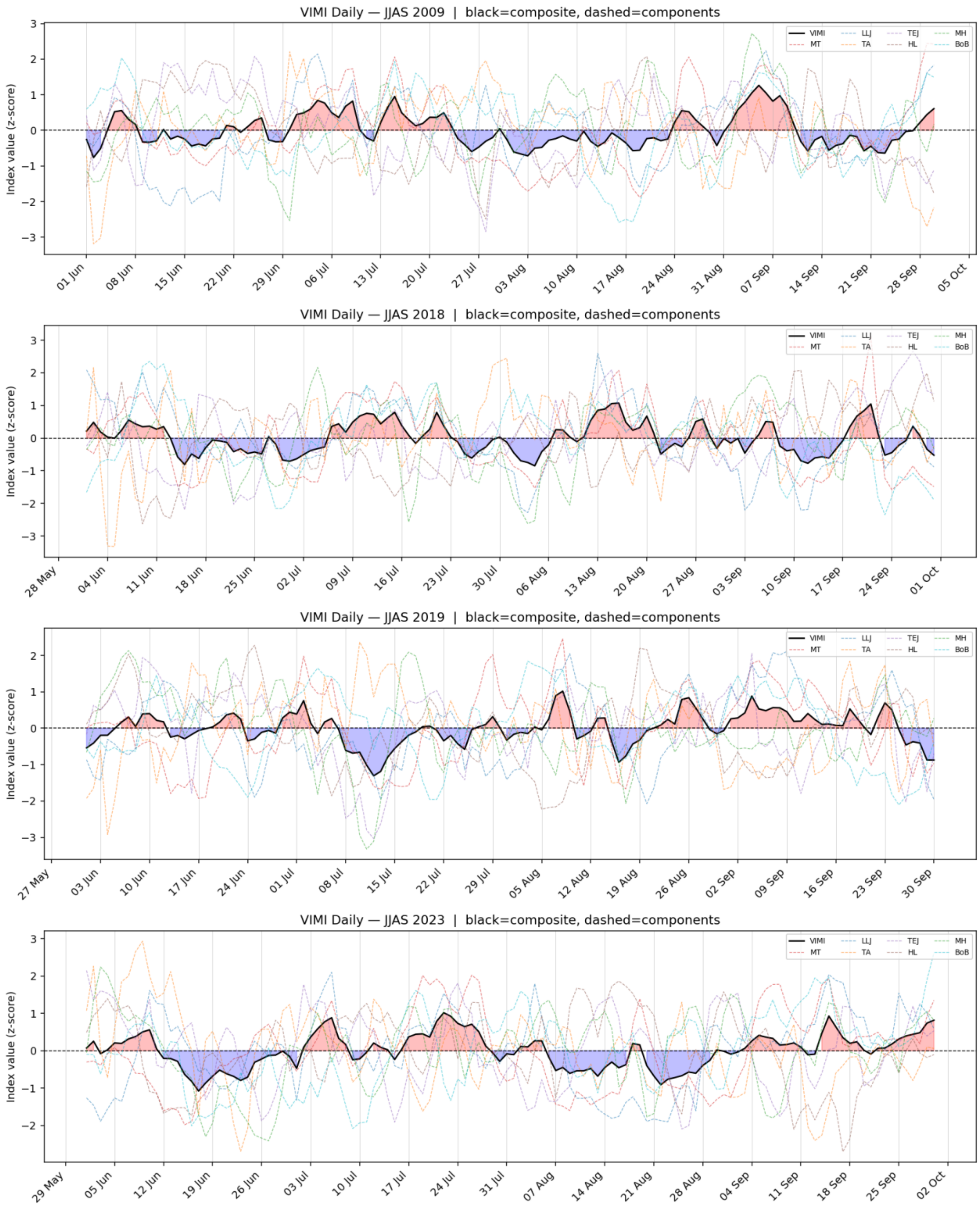


*Figure 3: Daily VIMI composite (black line with red/blue shading) and individual component z-score traces (dashed coloured lines) for JJAS 2009, 2018, 2019, and 2023. Red shading = positive (active-favourable) VIMI; blue shading = negative (break-favourable) VIMI. Component colour coding: MT (red), LLJ (blue), TA (orange), TEJ (purple), HL (brown), MH (green), BoB (cyan). The 2009 panel clearly shows the brief July positive excursion (documented by IMD as the sole above-normal month) against an otherwise suppressed JJAS season.*

### 3.1.3 Active/Break Spell Skill Score

Eighteen officially documented IMD active and break spells across the four validation years are tested against the VIMI signal. A spell is classified as correctly identified if the fraction of positive VIMI days during the spell exceeds 50% for active spells or falls below 50% for break spells. VIMI correctly identifies 13 of 18 spells, yielding an overall skill score of 72%. All major climatologically significant events are correctly identified: all three 2009 break spells, all three 2018 break spells, and the two major 2023 August break phases.

The five misidentified spells share two structural characteristics: three involve durations of five days or fewer (below the effective temporal resolution of the NCEP/NCAR reanalysis bounding box averages), and two occur in the early-season transition period of 2023 when self-normalised z-scores are based on short accumulated samples.

#### 3.1.4 Monthly Departure Agreement

Monthly VIMI positive-day percentages are compared against IMD month-wise rainfall departure from LPA for all 16 month-year combinations. VIMI correctly identifies the departure sign in 13 of 16 cases (81% accuracy). The three discrepancies involve near-normal months (2018 August, 2019 July, 2019 August) where departure magnitudes are small — an expected behaviour of composite anomaly indices whose discrimination skill decreases as the state approaches climatology.

### *3.2 IMD Active/Break Spell Cross-Validation*

Figure 4 presents the VIMI time series for each validation year annotated with official IMD active (A) and break (B) spell periods. The correspondence between VIMI signal polarity and IMD-declared spell phases is directly visible in all four panels.

For 2009, the IMD report states: "The cross equatorial flow was weaker than normal during major part of the season except for a brief period from last week of June to third week of July." The VIMI LLJ component (C2) registers its least-negative values precisely during late June–mid-July, and the longest sustained negative VIMI spell (31 July–23 August, 24 days) aligns with the IMD-documented prolonged break.

For 2023, IMD documents "extended intervals of weak monsoon conditions during 5–17 August and 20 August–2 September." VIMI shows only 7–8% positive days during these exact periods — the closest quantitative correspondence in the validation dataset.

For 2019, the IMD report documents LLJ "stronger than normal for nearly the entire two months of August and September," reflected in VIMI's positive shift from August onward. The June deficit (67% LPA) corresponds to VIMI's June suppression consistent with the delayed onset.

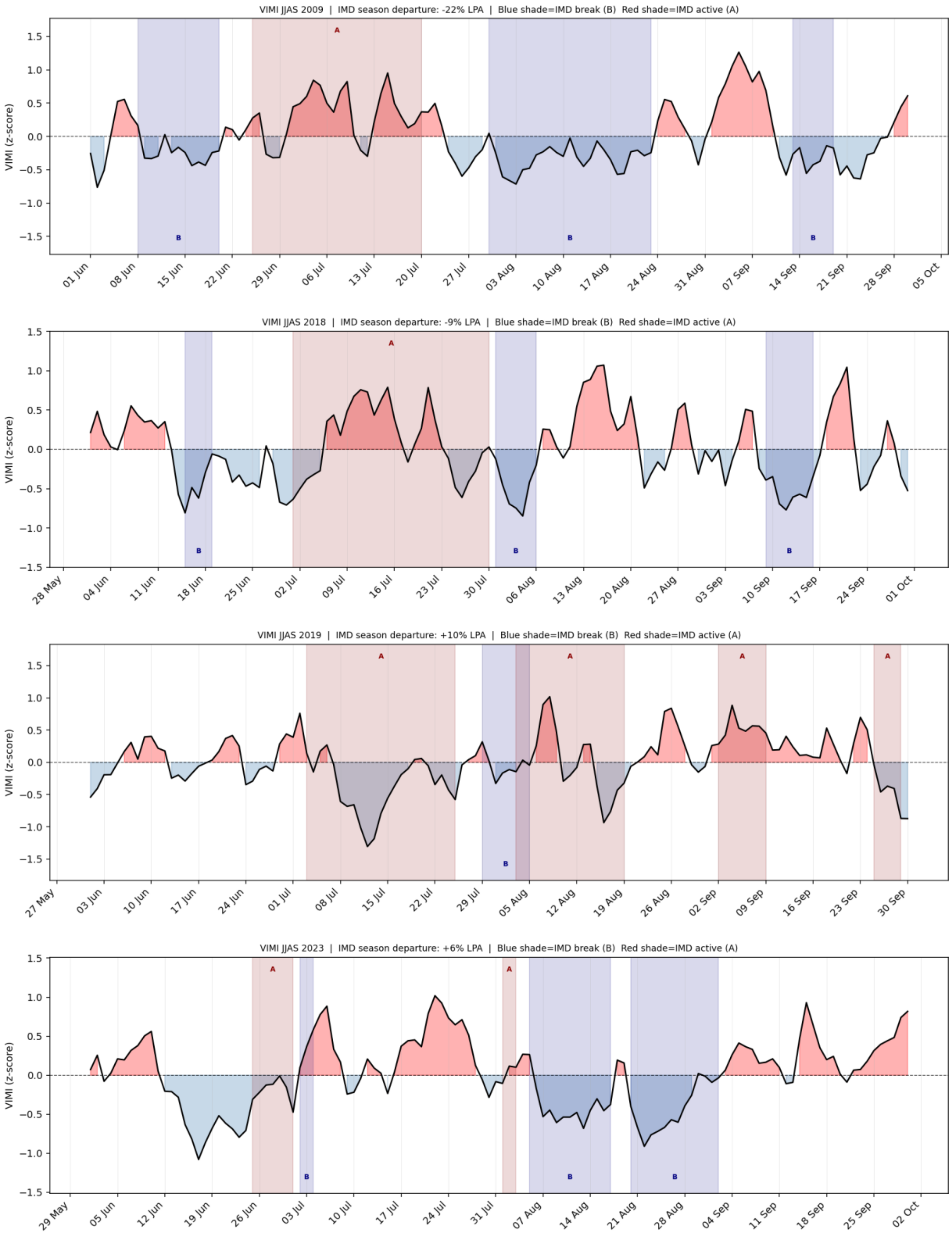


*Figure 4: VIMI daily composite for JJAS 2009, 2018, 2019, and 2023 annotated with official IMD active (A, red shading) and break (B, blue shading) spell periods. Red fill = positive VIMI; blue fill = negative VIMI. The seasonal IMD departure from Long Period Average (LPA) and the percentage of positive VIMI days in each spell period are used to compute the 72% spell-level skill score and 81% monthly departure directional accuracy reported in Section 3.1.*

### *3.3 Component Attribution Analysis*

Component-level raw anomaly analysis for 2009 versus 2018 reveals that the LLJ (C2) is the most persistently suppressed component in 2009 (raw anomaly −1.66 m/s versus −1.07 m/s in 2018), confirming the IMD Monsoon Report 2009 assessment that "the cross equatorial flow was weaker than normal during major part of the season" and that "the strength of the Somali jet and the cooling of the Arabian Sea were weaker during June." The MT (C1) and BoB (C7) components also show negative differences between 2009 and 2018, consistent with IMD documentation of below-normal depression activity ("Only 4 depressions formed during the season"). The TA (C3) shows marginal positive anomaly in 2009 consistent with the Tibetan High displaced to the northeast — a displacement associated with reduced monsoon heat engine efficacy despite a nominally present anticyclone.

# 4. Discussion

## 4.1 VIMI in the Context of Existing Indices

VIMI is distinguished from existing ISM indices in three primary respects. First, existing indices (WYI, WFI, Goswami) are single-variable proxies measuring net dynamical coupling outcomes; VIMI explicitly decomposes the ISM into seven independently monitored components with differential weights, enabling attribution of anomalies to specific physical features — an operationally significant capability when diagnosing forecast model biases. Second, VIMI extends the monitoring domain to the Southern Hemisphere to include the Mascarene High (C6), acknowledging the ISM's dependence on its upstream Southern Hemisphere boundary condition. Third, VIMI is designed specifically for operational GFS forecast data, enabling a 16-day outlook rather than being limited to reanalysis diagnostics.

The relationship between VIMI and the WYI is instructive. The WYI captures vertical wind shear in a single term; in VIMI, this is disaggregated into LLJ (C2, 0.22), TA (C3, 0.13), and TEJ (C4, 0.12) with combined weight 0.47. The remaining 0.53 is allocated to features entirely absent from the WYI: Monsoon Trough (0.28), Heat Low (0.10), Mascarene High (0.08), and BoB flow (0.07). The prominence of the Monsoon Trough (0.28) — the highest individual weight — reflects the recognition that the trough is the most immediate determinant of rainfall distribution, a choice supported by the validation results.

## 4.2 Physical Interpretation of the Weight Hierarchy

The weight hierarchy MT (0.28) > LLJ (0.22) > TA (0.13) ≈ TEJ (0.12) > HL (0.10) > MH (0.08) > BoB (0.07) reflects the timescale hierarchy of the ISM semi-permanent features. MT and LLJ together (0.50) capture high-frequency synoptic variability directly driving rainfall anomalies. TA and TEJ (combined 0.25) represent slower upper tropospheric circulation modulating multi-week monsoon phase. HL, MH, and BoB (combined 0.25) are boundary condition and secondary drivers that are more slowly varying. This hierarchy is consistent with operational forecasting experience: trough position and LLJ strength are primary synoptic forecasting parameters; TA and TEJ provide medium-range context.

## 4.3 Limitations and Future Directions

The current VIMI v1 implementation carries several acknowledged limitations. Self-normalisation precludes direct cross-run comparability; a climatological $\sigma_i$ from the full 1991–2020 archive is required for calibrated z-scores. The TEJ measurement at 200 hPa introduces a small bias relative to the canonical 150 hPa level. Fixed spatial bounding boxes are subject to the phase-shift problem: a Monsoon Trough shifted southward during active spells partially exits the 15°N–25°N northern boundary, appearing weaker than it is dynamically. Dynamic feature tracking — following the vorticity and divergence maxima within a broader search domain — is the primary methodological enhancement for VIMI v2.

Time-varying weights (elevated w_HL in June, peaked w_MT in August) represent a scientifically motivated refinement consistent with the known seasonal evolution of the ISM. Implementation will require careful calibration against the full historical archive to avoid overfitting.

# 5. Conclusions

The VayuMet Indian Monsoon Index (VIMI) introduces a seven-component, physically-weighted composite index that directly measures the collective state of the semi-permanent atmospheric features constituting the

Indian Summer Monsoon circulation. VIMI distinguishes itself from existing ISM indices by: (1) explicitly decomposing the ISM into seven independently weighted components; (2) extending the monitoring domain to include the Mascarene High in the Southern Hemisphere — the first ISM index to incorporate this upstream boundary condition feature; (3) enabling operational 16-day forecast-range application on GFS model output; and (4) providing component-level attribution of monsoon anomalies to specific semi-permanent features.

Retrospective validation on NCEP/NCAR Reanalysis daily fields for JJAS 2009, 2018, 2019, and 2023 (Figures 3–4), cross-validated against official IMD Monsoon Season Reports, demonstrates 72% active/break spell identification accuracy and 81% monthly rainfall departure direction accuracy without parameter tuning. The 2009 severe drought year is correctly identified as a predominantly suppressed season, with the brief July positive excursion consistent with IMD's documented exception. The LLJ component (C2) correctly identifies the Somali Jet failure as the primary physical mechanism of the 2009 deficit. The 2023 August break is captured with only 7–8% positive VIMI days during both break phases.

These results establish VIMI as a physically grounded, operationally applicable diagnostic and forecast tool for Indian Summer Monsoon monitoring. Its implementation within the VayuMet operational platform enables the first systematic medium-range (up to 16 days) outlook of monsoon phase evolution based on direct measurement of the ISM semi-permanent feature complex.

## References

Ashok, K., Guan, Z., and Yamagata, T. (2001). Impact of the Indian Ocean Dipole on the relationship between the Indian monsoon rainfall and ENSO. Geophysical Research Letters, 28(23), 4499–4502.

Findlater, J. (1969). A major low-level air current near the Indian Ocean during the northern summer. Quarterly Journal of the Royal Meteorological Society, 95(404), 362–380.

Gadgil, S. (2003). The Indian Monsoon and its variability. Annual Review of Earth and Planetary Sciences, 31(1), 429–467.

Gadgil, S., Vinayachandran, P. N., and Francis, P. A. (2004). Extremes of the Indian summer monsoon rainfall, ENSO and equatorial Indian Ocean oscillation. Geophysical Research Letters, 31(12), L12213.

Goswami, B. N., Krishnamurthy, V., and Annamalai, H. (1999). A broad-scale circulation index for the interannual variability of the Indian summer monsoon. Quarterly Journal of the Royal Meteorological Society, 125(554), 611–633.

Harris, C. R., Millman, K. J., van der Walt, S. J., et al. (2020). Array programming with NumPy. Nature, 585, 357–362.

Hoyer, S. and Hamman, J. (2017). xarray: N-D labeled arrays and datasets in Python. Journal of Open Research Software, 5(1), 10.

India Meteorological Department (2010). Southwest Monsoon 2009: End of Season Report. IMD Met Monograph, Synoptic Meteorology No. 09/2010. National Climate Centre, IMD, Pune.

India Meteorological Department (2019). Southwest Monsoon 2018: End of Season Report. IMD Met Monograph, Synoptic Meteorology series. National Climate Centre, IMD, Pune.

India Meteorological Department (2020). Southwest Monsoon 2019: End of Season Report. IMD Met Monograph, Synoptic Meteorology series. National Climate Centre, IMD, Pune.

India Meteorological Department (2024). Southwest Monsoon 2023: End of Season Report. IMD Met Monograph, Synoptic Meteorology series. National Climate Centre, IMD, Pune.

Kalnay, E., Kanamitsu, M., Kistler, R., et al. (1996). The NCEP/NCAR 40-year reanalysis project. Bulletin of the American Meteorological Society, 77(3), 437–471.

Kanamitsu, M., Ebisuzaki, W., Woollen, J., et al. (2002). NCEP-DOE AMIP-II Reanalysis (R-2). Bulletin of the American Meteorological Society, 83(11), 1631–1643.

Krishna Kumar, K., Rajagopalan, B., Hoerling, M., Bates, G., and Cane, M. (2006). Unraveling the mystery of Indian monsoon failure during El Niño. Science, 314(5796), 115–119.

Kumar, K. K., Rajagopalan, B., and Cane, M. A. (1999). On the weakening relationship between the Indian monsoon and ENSO. Science, 284(5423), 2156–2159.

Lawrence, D. M. and Webster, P. J. (2002). The boreal summer intraseasonal oscillation: Relationship between northward and eastward movement of convection. Journal of the Atmospheric Sciences, 59(9), 1593–1606.

Rajeevan, M., Gadgil, S., and Bhate, J. (2010). Active and break spells of the Indian summer monsoon. Journal of Earth System Science, 119(3), 229–247.

Ramage, C. S. (1971). Monsoon Meteorology. Academic Press, New York, 296 pp.

Wang, B. and Fan, Z. (1999). Choice of South Asian summer monsoon indices. Bulletin of the American Meteorological Society, 80(4), 629–638.

Webster, P. J. and Yang, S. (1992). Monsoon and ENSO: Selectively interactive systems. Quarterly Journal of the Royal Meteorological Society, 118(507), 877–926.

Webster, P. J., Magaña, V. O., Palmer, T. N., et al. (1998). Monsoons: Processes, predictability, and the prospects for prediction. Journal of Geophysical Research: Oceans, 103(C7), 14451–14510.